ACS Biomaterials SCIENCE & ENGINEERING
Cite This: ACS Biomater. Sci. Eng. XXXX, XXX, XXX−XXX
Article
pubs.acs.org/journal/abseba

High-Performance Intraocular Biosensors from Chitosan-Functionalized Nitrogen-Containing Graphene for the Detection of Glucose

Ruitao Zou,[†,‡] Suyan Shan,[†,‡] Libin Huang,[†,‡] Zhi Chen,[§] Tom Lawson,[∥] Mimi Lin,[†,‡] Lu Yan,*[,†,‡] and Yong Liu*[,†,‡]

[†]Laboratory of Nanoscale Biosensing and Bioimaging, School of Ophthalmology and Optometry, School of Biomedical Engineering, Wenzhou Medical University, 270 Xueyuanxi Road, Wenzhou, Zhejiang 325027, China

[‡]State Key Laboratory of Ophthalmology, Optometry, and Vision Science, Wenzhou Medical University, Wenzhou, Zhejiang 325027, China

[§]ARC Centre of Excellence for Electromaterials Science, Intelligent Polymer Research Institute, AIIM Facility, University of Wollongong, Squires Way, Wollongong, New South Wales 2522, Australia

[∥]ARC Centre of Excellence for Nanoscale Biophotonics (CNBP), Department of Physics and Astronomy, Macquarie University, 7 Wally's Walk, Sydney, New South Wales 2109, Australia

Supporting Information

ABSTRACT: The noninvasive and real-time detection of glucose sugar from tears is promising for the early diagnosis and treatment of chronic diseases such as diabetes. However, its realization is a big challenge. A suitable biosensor electrode that can closely fit the eye and be electrochemically sensitive is still unrealized. In this work, nitrogen-doped graphene (N-G) was used as an ophthalmic electrode in a high-performance intraocular biosensor. The use of N-G has been reported elsewhere before as it is highly electroactive and so has a particular use in biosensors. We hereby present a novel procedure for making carboxylated chitosan-functionalized nitrogen-containing graphene (GC−COOH) by using a one-step ball-milling process. This process does not use toxic chemicals, flammable gases, or a high temperature. It is thus particularly easy to perform. The fabricated nanomaterial had a high electroactivity and was easily assembled as a glucose biosensor by the immobilization of glucose oxidase. The thus constructed biosensor has a high sensitivity at 9.7 μA mM^{-1} cm^{-2}, a broad linear range at 12 mM, and a good detection limit of 9.5 μM. It was able to maintain this activity after a month of storage. We also report the intraocular use of this constructed biosensor. The as-prepared GC−COOH was found to be highly biocompatible to ophthalmologic cells such as corneal epithelial and retinal pigment epithelium cells. No change in the intraocular pressure or the corneal structure was measured in a New Zealand white rabbit model. The as-assembled sensor was worn by the animals for more than 24 h without undue impact. This result confirmed the biosensor's potential for intraocular application in the clinic. Its assembly into a useful sensor shown here has great potential to provide real-time monitoring of glucose levels in tear fluids of patients with high sugar levels.

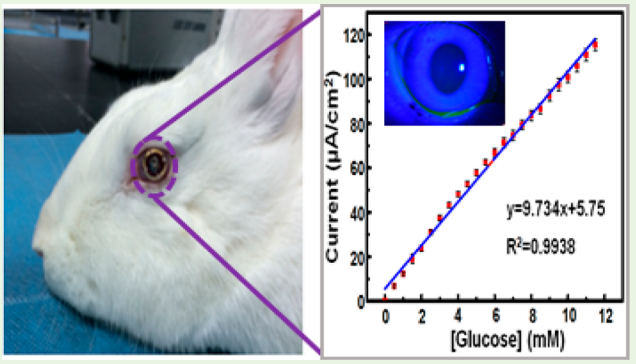

KEYWORDS: *glucose, intraocular wearable biosensors, nitrogen-doped graphene, corneal epithelial cells, retinal pigment epithelium cells*

INTRODUCTION

Diabetes is the third most frequent chronic disease.[1] 25% of patients with diabetic retinopathy eventually become blind.[2] Its early diagnosis and treatment are essential. The level of a person's blood glucose is a sign of diabetes.[3] Hence, real-time detection and accurate monitoring of glucose levels are important. Various types of glucose biosensors, especially electrochemical biosensors, were reported.[4,5] Some electrochemical biosensors were based on traditional metals (such as gold and platinum) and reported good sensing performance for blood glucose detection. Noninvasive and real-time detection of glucose from other body liquids such as tears are, however, still a challenge. Metal-based electrodes have more limited sensing sensitivity and biocompatibility. The glucose content in tears is consistent with levels of sugar in blood.[6] Thus, noninvasive biosensors based on tear glucose can be used for

Received: July 29, 2019
Accepted: December 4, 2019

DOI: 10.1021/acsbiomaterials.9b01149
ACS Biomater. Sci. Eng. XXXX, XXX, XXX−XXX

the real-time detection of glucose. The rapid development of graphene-based nanomaterials[7−9] has provided an opportunity for the development of novel glucose biosensors. In particular, nitrogen-doped graphene is a useful material for the fabrication of novel biosensors. The high electroactivity of nitrogen-doped graphene (N-G) and its use in biosensors have been reported elsewhere.[10−13] Within N-G, the introduction of the electron withdrawing atom, nitrogen, into the sp^2-hybridized carbon matrix creates a net positive charge on the adjacent Π−Π conjugated carbon atoms. This provides an active carbon site for electrochemical reactions to occur.[14−16] The addition of nitrogen-containing molecules such as nitrobenzene and polyaniline onto the surface of graphene without damaging the integrity of its matrix can also prepare a highly electroactive electrode.[17,18] However, the preparation of N-G-based materials can involve complicated chemical redox processes that are not easily scalable.[19−21]

In this work, a facile and environmentally friendly method to prepare biocompatible and electroactive N-G-based nanomaterials was used as a biosensor electrode. The N-G was prepared by adding a graphite and biocompatible nitrogen-containing polymer, chitosan, to an edge-functionalized ball-milling process.[22] Milling was carried out at room temperature, at normal pressure, and without the addition of other chemicals. Chitosan is a deacetylated form of chitin, a material found in crab exoskeleton. Chitosan was reported elsewhere in many biomedical applications as it has high biocompatibility, biodegradability, and can interact with bioactive molecules such as antibody and enzyme.[23] Carboxylated chitosan (such as carboxymethylated chitosan) possesses similar properties, but it has a much higher hydrophilicity. It can be more readily used in biomedical applications where biocompatibility, antibacterial activity, and film-forming are needed.[24] In the present work, the incorporation of carboxymethylated chitosan with graphene is reported, and the resulting N-G electrode was potentially used for the real-time detection of glucose from tears.

EXPERIMENTAL SECTION

Reagents and Materials. Carboxymethylated chitosan and N-(3-(dimethylamino)propyl)-*N*′-ethylcarbodiimide hydrochloride (EDC) were provided by Aladdin Chemistry Corporation. Graphite flakes were obtained from Qingdao Haida Corporation. Fetal bovine serum (FBS), trypsin, and Dulbecco's modified Eagle's medium (DMEM) were purchased from Invitrogen Corporation. A CellCounting Kit-8 assay (CCK-8) was bought from Dojindo Molecular Technologies, Inc. Glucose oxidase (type VII, lyophilized powder, ≥100 units mg^{-1}, from *Aspergillus niger*), D-(+)-glucose and *N*-hydroxysuccinimide (NHS) were supplied by Sigma-Aldrich. Phosphate buffer saline was bought from Fuzhou Maixin Biotech. Indium tin oxide (ITO)-coated glass was received from Zhuhai Kavio Optoelectronic Technology Corporation.

Preparation of Carboxyl-Chitosan-Functionalized Nitrogen-Containing Graphene. Carboxyl-chitosan-functionalized nitrogen-containing graphene (GC−COOH) was prepared by ball-milling a mix of graphite flakes and carboxymethylated chitosan at a mass ratio of 1:5 (w/w). The mixture was vigorously milled at a rate of 400 rpm for 8 h using a planetary ball-mill (Nanjing Nanda Instrument Plant), followed by its centrifugation in deionized (DI) water at 500 rpm for 10 min to remove any unbound graphite in the lower precipitation. The as-obtained materials were further centrifuged at 3000 rpm for 10 min to clear remaining impurities such as unreacted chitosan in the upper liquid. The precipitate was dispersed in DI water and then placed in a dialysis bag overnight for further removal of any impurities.

Preparation of the Enzyme Electrode. A glass carbon electrode (GCE, i.d. = 3 mm) was pretreated with DI water and ultrasonication for 15 min. A 5 μL portion of GC−COOH (4 mg mL^{-1} in DI water) was then cast onto the GCE and dried at 50 °C in air. The electrode was subsequently soaked in a PBS solution (0.1 M, pH = 7.4), which comprised 0.015 M *N*-hydroxyl succinimide (NHS), 0.03 M 1-ethyl-3-(3-dimethylaminoprophy)-carbondiimide hydrochloride (EDC), and 10 mg mL^{-1} glucose oxidase (GOx), for 60 min to immobilize the GOx in the GC−COOH via an amidation reaction. The carboxyl groups of GC−COOH formed from carboxyl-chitosan covalently immobilize the amine groups of GOx. A GC−GOx enzyme electrode was thus prepared. The enzyme electrode was then rinsed with PBS (0.1 M, pH = 7.4) three times to remove unreacted GOx.

For better differentiation of the biosensing signals from the enzyme electrode, an ITO glass slide (1 × 5 cm^2) precoated with Pt was used as the substrate for the deposition of the enzyme. The ITO glass slide was ultrasonicated in acetone and rinsed in DI water prior to its use. A thin layer of Pt was further coated onto the glass slide using a Sputter Coater set at 100 mA for 60 s. A 200 μL portion of GC−COOH (4 mg mL^{-1}) was spin-coated onto the slide and dried at room temperature in air. Finally, the resulting electrode was soaked in the PBS solution (0.1 M, pH = 7.4), which contained 0.015 M NHS, 0.03 M EDC, and 10 mg mL^{-1} GOx, for 60 min. The enzyme electrode was rinsed with a PBS solution (0.1 M, pH = 7.4) three times before testing.

Cell Culture. Healthy human ocular cells such as ARPR-19 cells (at a density of 5000 cells per well) were preincubated in a 96-well plate for 24 h. The as-synthesized GC−COOH set at various concentrations (0, 5, 25, 50, and 100 μg mL^{-1}) were mixed with a DMEM/F12 medium. 10% FBS was added to the precultured ARPR-19 cells. A Cell Counting Kit-8 (CCK-8) assay[25] identified the cell survival rates after their exposure to the GC−COOH over various time periods. Cells were then cultured in an incubator containing 95% air/5% CO_2 at 37 °C.

Intraocular Biosensors. A corneal contact electrode (Fabrinal), used for electroretinogram testing, was applied as the substrate for the formation of intraocular biosensors. As shown in Figure 3c, a gold circle layer was presented on the corneal contact electrode to provide good conductivity, and four connection sites were left on its back for the fast delivery of electrical signals. A circle with 0.3 mm diameter in the center of the electrode was then sputter-coated with platinum. The GC−GOx dispersion was placed onto the Pt area and then dried in air. This intraocular biosensor was then tested by wearing on the eye.

***In Vivo* Experiments.** Five New Zealand white rabbits with an average weight of 2.5−4 kg were used as a model for the *in vivo* tests. Regular ocular examinations, such as slit-lamp examination and ophthalmoscopy, were carried out on the rabbits to make sure they were healthy. Intraocular pressure (IOP) was measured using a Tono-Pen instrument (Mentor Tono-pen XL Medtronic Solan, America). Corneal structure damage was tested with a fluorescein sodium staining test paper using slit-lamp microscopy with a cobalt-blue light.

Characterization. The electrochemical measurement was performed with a CHI 760D electrochemical workstation. A Ag/AgCl (in saturated KCl) electrode was applied as the reference electrode with a Pt wire counter electrode. A Bruker MultiMode 8 microscope (in a tapping mode) measured the morphology of the nanomaterials. Physiochemical properties of the fabricated materials were determined with a Spectrum One FTIR spectrometer (PerkinElmer), a model OCA15EC contact angle goniometer (Dataphysics), a Cary-100 UV spectrometer (Aligent), a multifunctional X-ray photoelectron spectroscope (Shimadzu), a D8 Advance X-ray diffraction spectrometer (Bruker), a Nicolet Almega Raman spectroscope (Thermal Fisher Scientific), and an Advance III HD 500 MHz nuclear magnetic resonance (NMR) spectrometer (Bruker BioSpin), respectively.

Ethical Conduct of Research. The authors state that they have obtained approval from the Wenzhou Medical University Animal Care and Use Committee for the animal tests. All tests on the animals carried out and reported in this work followed the principles outlined

DOI: 10.1021/acsbiomaterials.9b01149
ACS Biomater. Sci. Eng. XXXX, XXX, XXX−XXX

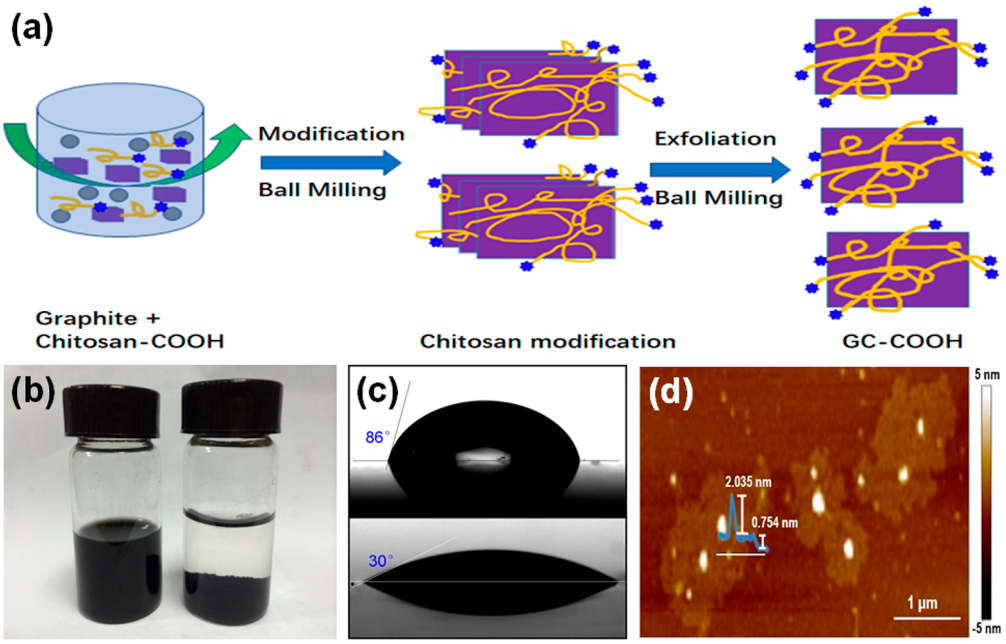

Figure 1. Preparation and characterization of carboxyl-chitosan-functionalized nitrogen-containing graphene (GC−COOH). (a) Schematic synthesis of GC−COOH. The blue stars indicate carboxyl groups. (b) Digital image of (left) the as-synthesized GC−COOH dispersed in DI water, compared to (right) a corresponding graphite after ball-milling. (c) Water contact angle of (top) a hydrophobic CD plate and (bottom) the same CD plate coated with a layer of GC−COOH. (d) AFM micrograph of the obtained GC−COOH.

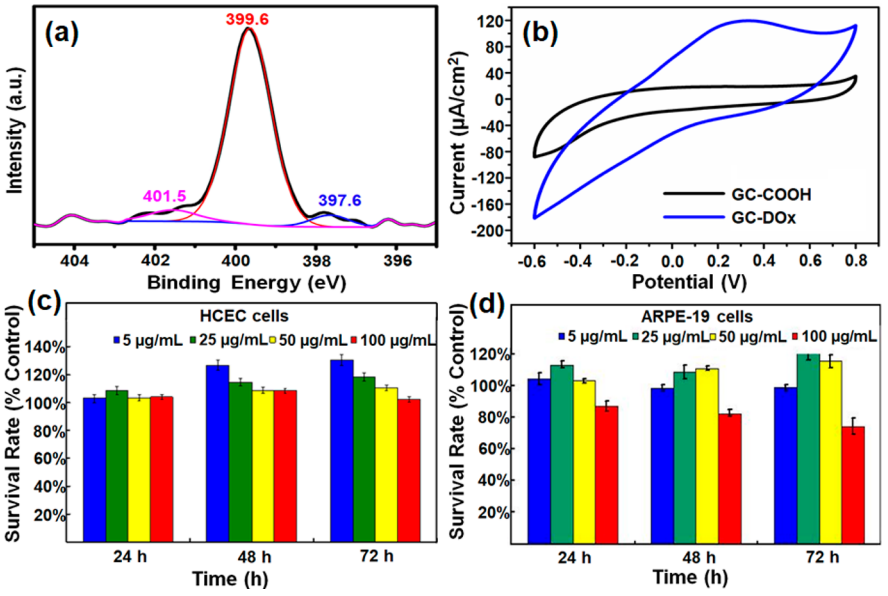

Figure 2. Physiochemical characterization and cytotoxicity measurement on GC−COOH. (a) High-resolution N 1s spectrum of GC−COOH. (b) Cyclic voltammograms obtained at NG/GCE (black), GOx/NG/GCE (red), and GOx/NG/GCE with addition of 10 mM glucose in 0.1 M PBS (pH = 7.4) buffer solution at 100 mV s^{-1} scan rate. (c) CCK-8 cell survival rate of HCECs incubated with various GC−COOH amounts. (d) CCK-8 cell survival rates of ARPE-19 cells cocultured with different GC−COOH amounts.

in the Declaration of Helsinki for all human or animal experimental investigations.

RESULTS AND DISCUSSION

The formation of the carboxyl-chitosan-functionalized nitrogen-containing graphene (GC−COOH) nanosheets is schematically shown in Figure 1a. Graphite and carboxyl-chitosan, as detailed in the Experimental Section, were mixed in a sealed capsule and vigorously shaken so that mechanical exfoliation of graphene nanosheets occurred. Initially, carboxyl-chitosan was functionalized on the edge of graphite sheets via a solid-phase mechanochemical reaction.[26] This added chitosan expanded the layered space between graphite sheets and decreased the corresponding bond energy of covalent bonds connecting the graphite layers. Along with the applied milling force, this broke the connecting bonds between the graphite layers and exfoliated these layers into nanosheets along the shear-force of milling. Figure 1b shows the as-synthesized GC−COOH dispersed evenly in DI water. The uniform dispersion of GC−COOH in water stayed intact after 1 month of storage in air. In

DOI: 10.1021/acsbiomaterials.9b01149
ACS Biomater. Sci. Eng. XXXX, XXX, XXX−XXX

contrast, ball-milled graphite samples not containing chitosan never dispersed well in water, as shown in Figure 1b. This provided another confirmation that water-soluble carboxyl-chitosan was successfully incorporated with graphene nanosheets after the ball-milling treatment. The strong hydrophilicity of GC−COOH was again confirmed by running a water contact angle analysis, and this is shown in Figure 1c. The pristine CD substrate had an air−water contact angle of 86°, and this confirms its hydrophobic surface. The hydrophilicity of the CD surface was enhanced significantly, and the contact angle was decreased to 30°, after a layer of GC−COOH was coated to its top. The micromorphology of GC−COOH was measured using atomic force microscopy (AFM). Typically, shaped nanoscale flakes with an average thickness of 0.75 nm were observed (Figure 1d), indicating that the as-synthesized GC−COOH comprised single or a few layered nanosheets. Additionally, presence of chitosan on the nanosheets was evident in the AFM image. The morphology of GC−COOH was further measured using transmission electronic microscopy (TEM). As shown in Figure S1, a typical nanoscale flakelike shape with the presence of chitosan particles is visible in the TEM micrograph of GC−COOH.

The physiochemical properties and molecular structures of the as-prepared GC−COOH were characterized using various techniques. The XPS results of GC−COOH are shown in Figure 2a and in Figure S1. The XPS survey spectrum (Figure S1a) showed that there are three elements (O, N, and C) present in the GC−COOH. The nitrogen content in GC−COOH was 4.6%. As can be seen in Figure 1a, the high-resolution N 1s spectrum was fitted to three peaks. The predominant peak at 399.6 eV was attributed to the nitrogen in chitosan, which was also observed in the N 1s spectrum of pristine chitosan. Two peaks at 397.6 and 401.5 eV indicated pyridinic N and quaternary N, respectively. It was reported that pyridinic N demonstrated good activity in electrochemical reactions[27] and in electrochemical biosensing.[10] The presence of pyridinic N in GC−COOH may provide electroactive sites for GC−COOH. Figure S2b is the high-resolution C 1s spectrum of GC−COOH fitted to three main peaks. These include C═C at 284.8 eV, C—O at 286.2 eV, and the sp^3 carbon bonded with N and O at 287.9 eV. The high-resolution O 1s spectrum in Figure 1c indicated a C═O at 531.2 eV and a C—O at 532.6 eV, respectively. XPS spectra confirmed the presence of carboxyl groups and nitrogen-containing groups (e.g., pyridinic N) in the GC−COOH that was formed. This supports the successful functionalization of chitosan with graphene.

A Raman spectrum of GC−COOH in Figure S3 indicates three characteristic peaks of graphene-based nanomaterials: the D band at 1361 cm^{-1} associated with the sp^3-hybridized carbon (i.e., disorders and defects), the G band at 1596 cm^{-1} indicating the sp^2 carbon, and the 2D band at 2714 cm^{-1} attributed to the two phonon intervalley double resonance scattering. The peak intensity ratio of the D band to the G band (I_D/I_G) indicates the defect density of the graphene-based nanomaterials. In this work, I_D/I_G of GC−COOH was 0.83, compared to 0.5 for hydroxyl-graphene that was fabricated using a solid ball-milling method.[22] This suggests that the chitosan polymer introduced more defects into the graphene matrix than that caused by the hydroxyl groups present. Figure S4 shows the FTIR spectra of GC−COOH, pristine carboxyl-chitosan, and graphite after milling. Most characterization peaks of carboxyl-chitosan (red, Figure S4) were observed at the spectrum of GC−COOH (the blue curve, Figure S4). As shown in the GC−COOH spectrum, a broad band at 3417 cm^{-1} is associated with the overlapped stretching vibration of N—H and —OH. Two peaks obtained at 1577 and 1404 cm^{-1} indicate carboxyl-functional groups. A peak at 1047 cm^{-1} is attributed to the stretching vibration of C—N. No such band in the spectrum of graphite was observed after milling. The FTIR result confirmed the incorporation of nitrogen-containing chitosan with graphene. We further measured the ^{13}C solid NMR spectrum of GC−COOH as shown in Figure S5. The typical resonance at 120 ppm is attributed to the sp^2-hybridized carbon, which was predominant in the graphene matrix. Three characteristic peaks of carboxyl-chitosan were seen in the GC−COOH spectrum. A peak at 175 ppm (from the C═O), 74 ppm (originated from the C—O), and 31 ppm (associated with alkane), respectively. This further confirmed GC−COOH synthesis.

The electrochemical property of GC−COOH was measured by cyclic voltammograms (CVs) in 0.1 M PBS solution (pH = 7.4) and with the addition of 5 mM glucose. As shown in Figure 2b, no redox peak was observed, but capacitive currents were seen at the CV of the pristine GC−COOH (black curve, Figure 2b). This suggests significantly enhanced electroactivity of the electrode, when nitrogen-containing polymer (i.e., chitosan) was added to the graphene matrix. When a GOx immobilized GC−COOH enzyme electrode was applied, a well-defined anodic peak due to the oxidation of glucose by GOx was visible at 0.3 V (blue curve, Figure 2b). This confirmed the covalent linkage between GC−COOH and GOx, and rapid response of the as-synthesized GC−GOx enzyme electrode.

The ocular biocompatibility of GC−COOH is an important consideration for clinical biosensors, especially in ophthalmology. We investigated the ocular biocompatibility *in vitro* by the use of ocular cells such as corneal epithelial cells (CECs) and retinal pigment epithelium (RPE) cells. Human CECs (HCECs) were used to test the biocompatibility of the ocular surface, while ARPE-19, a cell line derived from human RPE, tested the cytotoxicity of the fundus. As shown in Figure 2c, HCEC viabilities were observed to be higher than 100% when the concentration of GC−COOH tested was varied from 5 to 100 $\mu g\ mL^{-1}$. The cell viabilities remained above 100% when the coculture time was increased from 24 to 72 h. This suggests that the addition of GC−COOH is beneficial for the growth and proliferation of HCECs. Since the designed intraocular biosensor can be worn on the cornea, intimate contact between them is inevitable. The cell viability results seen here support the safe use of intraocular wearable biosensors based on a GC−COOH electrode. When ARPE-19 cells were cocultured with various amounts of GC−COOH nanomaterials (Figure 2d), the cell viabilities were found to be higher than 100% when the concentration of GC−COOH was less than 50 $\mu g\ mL^{-1}$, and it was cultured over 24−72 h. The cell survival rate of ARPE-19 cells remained above 80% when 100 $\mu g\ mL^{-1}$ GC−COOH was applied. The GC−COOH induced cell viability of ARPE-19 cells is much higher than that seen when the graphene oxide (which is the most popular applied graphene derivative in the fields of biosensors and biomedicine) was reported. As reported elsewhere, the induced cell survival rate of ARPE-19 cells is above 60%.[28] This suggests that GC−COOH can be a better graphene-based nanomaterial for ophthalmic applications. Overall, *in vitro* cytotoxicity testing results reported here confirm the high

DOI: 10.1021/acsbiomaterials.9b01149
ACS Biomater. Sci. Eng. XXXX, XXX, XXX−XXX

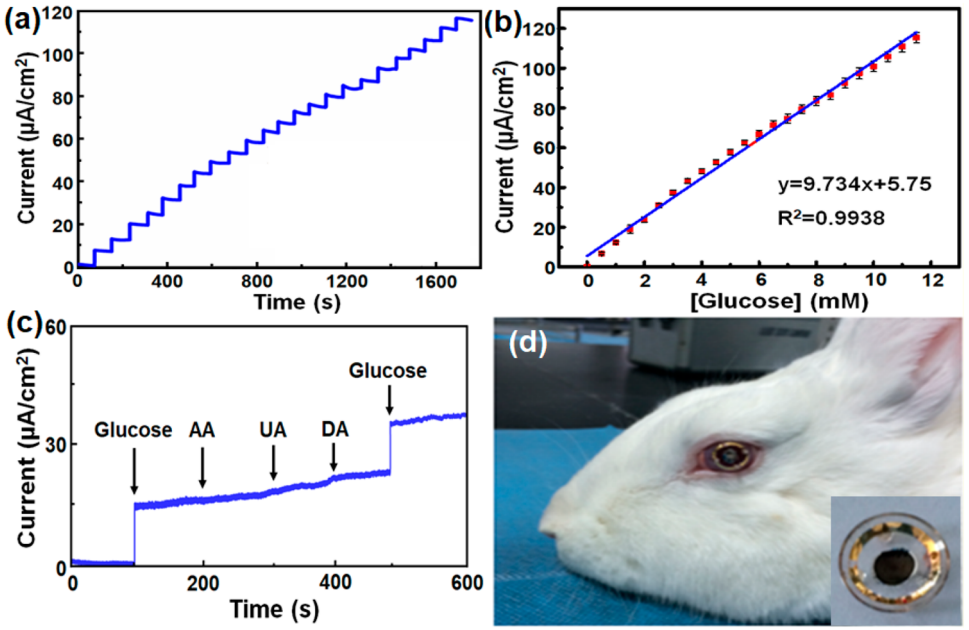

Figure 3. Biosensing performance of the as-prepared GC−COOH based biosensor. (a) Amperometric response of the GC−GOx enzyme electrode to the successive additions of 0.5 mM glucose at +0.5 V vs Ag/AgCl in 0.1 M PBS (pH = 7.4). (b) Calibration curve obtained for glucose detection. (c) Amperometric response of the GC−GOx enzyme electrode to the addition of 1 mM glucose, 50 mM uric acid, 50 mM ascorbic acid, and 50 mM dopamine at +0.5 V vs Ag/AgCl in 0.1 M PBS (pH = 7.4). (d) Intraocular biosensor made from GC−COOH worn on a rabbit's cornea. The inset in part d shows the working side of the intraocular biosensor.

biocompatibility of GC−COOH with ocular cells. This indicates the safe use of GC−COOH-based electrodes in ophthalmic areas.

Amperometric measurement of a GC−GOx electrode after the successive addition of glucose to 0.1 M PBS was tested. A constant potential (0.5 V vs Ag/AgCl), where hydrogen peroxide created by the oxidation of glucose became oxidized, was applied to the enzyme electrode. Figure 3a shows the current responses at the enzyme electrode with the consecutive addition of 0.5 mM glucose in 0.1 M PBS solution. An oxidation current at the GC−GOx electrode was observed when glucose was introduced. No such current response was seen when a pristine GC−COOH electrode was tested without the presence of GOx. This confirmed that the current response seen could be attributed to the oxidation of hydrogen peroxide during the enzyme reaction. The positive current increased linearly with the successive addition of 0.5 mM glucose. A linear relationship between the oxidation currents and accumulative glucose concentrations (R^2 = 0.9938) was seen in the calibrated curve in Figure 3b. The sensitivity of the as-synthesized GC−COOH-based biosensor was 9.7 μA mM^{-1} cm^{-2}, calculated from the slope of the calibrated curve. The current response was linear up to 12 mM glucose. The detection limit of the GC−COOH-based biosensor was 9.5 μM.

The sensing performance of the resulting biosensor may be interfered by other physiologically active materials—such uric acid (UA), ascorbic acid (AA), and dopamine (DA)—in tear fluids. The biosensor's selectivity on the glucose detection was thus tested. As shown in Figure 3c, it was found that the sensing current at the enzyme electrode increased significantly with the addition of just 1 mM glucose. No change occurred when other materials (such as 50 mM UA, 50 mM AA, and 50 mM DA) were added. These results confirmed the high selectivity of the glucose biosensor.

We further measured the reproducibility of the resulting biosensor by testing 5 parallel enzyme electrodes. Five different enzyme electrodes were prepared using the same method and tested under preidentified conditions, separately. Their biosensing performance is shown in Figure S6. A high reproducibility with a small relative deviation (RSD) of 3.4% was achieved. The repeatability of the biosensor was identified by testing the GC−GOx electrode in 5 different glucose (5 mM) solutions. A small RSD of 4.7% was obtained. The long-term stability of the as-synthesized biosensor was established after storing the enzyme electrode at 4 °C over 1 month. Sensitivity of the biosensor decreased by only 25% after this storage. This decrease may be due to the inevitable deactivation of GOx after long-term storage.

To test the ophthalmologic use of the biosensor, we manufactured an intraocular biosensor from GC−GOx using a process described in the Experimental Section. As shown in Figure 3d, the as-prepared intraocular biosensor was formed from a flexible and transparent corneal contact electrode. The corneal electrode was easily worn on the rabbit's cornea. Glucose contents in tear fluids (if any) could be monitored using the intraocular biosensor by transferring the current signals from the oxidation of glucose by GOx into the external recorder via the gold layer on the corneal electrode. Real-time detection might be achievable, and this is shown in Figure S7. Measured changes in the glucose content of tear fluids could be recorded by the electrochemical station. However, workable *in vivo* real-time biosensing is dependent on resolving many issues. For example, in animal models that have high blood sugar, the generation of sufficient amounts of tear fluids is still an issue. The sensing sensitivity is also dependent on the quietness of the animal and the stability of the signal transmission when the animal is blinking. Further studies are needed to develop a workable device that does real-time monitoring. Instead, we monitored the glucose content in

DOI: 10.1021/acsbiomaterials.9b01149
ACS Biomater. Sci. Eng. XXXX, XXX, XXX−XXX

artificial tears (Hycosan, EUSAN) using the intraocular biosensor we prepared in this work. As shown in Figure S8, the sensing current is sensitive to the varied glucose content in the artificial tears. This supports that the as-prepared intraocular biosensor has the potential to real-time monitor the blood sugars in tear fluids in the future.

We further measured the *in vivo* ocular impact of the biosensing electrodes on ocular tissues. This could indicate directions for future work on the future development of intraocular devices. These include the influence of wearing the biosensing electrode on the corneal structure and the intraocular pressure (IOP) of animal models. As shown in Figure 4, both the microscopy image and fluorescein sodium stained image had no significant difference in the corneal surface structure of the rabbits wearing or not wearing the GC-based biosensor over 24 h. The corneal surface remained clear and transparent for both the treated group and the control. There was no obvious congestion and inflammatory reaction observed. The as-synthesized intraocular biosensor has a high biocompatibility to the vision system. Table S1 summarizes the IOP changes to rabbits wearing the GC-based biosensor over various time periods. The IOP across these time periods did not change.

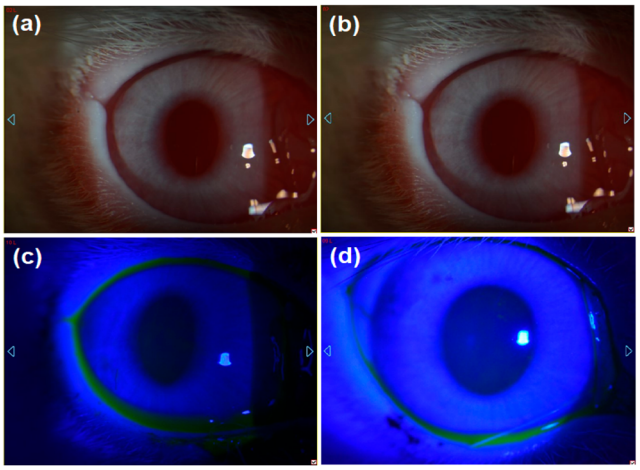

Figure 4. *In vivo* ocular impact of the biosensing electrode. Corneal surface of the experimental rabbit (a) before and (b) after wearing the GC-based biosensor over 24 h; the fluorescein sodium stained corneal surface of the rabbit (c) before and (d) after wearing the GC-based biosensor over 24 h.

CONCLUSIONS

In this work, a facile and efficient approach to prepare a highly electroactive and biocompatible nitrogen-containing polymer (e.g., chitosan) doped grapheme using an edge-functionalized ball-milling technique was demonstrated. The as-synthesized chitosan-graphene nanomaterial had the properties necessary for a high-performed biosensing electrode. Glucose biosensors based on this chitosan-graphene showed a high sensitivity, broad linear range, and good detection limit and remained stable after long-term storage. The electrode was further tested on an animal model as an assembled wearable corneal contact electrode for the real-time monitoring of intraocular blood sugar in tears. The chitosan-graphene showed a high biocompatibility with normal ocular cells such as corneal epithelial cells and retinal pigment epithelium cells. The as-assembled intraocular biosensor had no inverse impact on both the corneal structure and the intraocular pressure. This supports its use for the real-time detection of glucose levels in tears.

ASSOCIATED CONTENT

Supporting Information

The Supporting Information is available free of charge at https://pubs.acs.org/doi/10.1021/acsbiomaterials.9b01149.

TEM, XPS spectra, Raman spectra, FTIR spectra, solid-state ^{13}C NMR spectra, reproducibility results, biosensing performance using the intraocular biosensor, and intraocular pressure changes (PDF)

AUTHOR INFORMATION

Corresponding Authors

*E-mail: yanlu2017@wmu.edu.cn.
*E-mail: yongliu1980@hotmail.com.

ORCID

Lu Yan: 0000-0002-1851-1576
Yong Liu: 0000-0001-6932-583X

Author Contributions

The manuscript was written through contributions of all authors. All authors have given approval to the final version of the manuscript.

Notes

The authors declare no competing financial interest.

ACKNOWLEDGMENTS

This research was funded by the National Key R&D Program of China (2018YFA0107304), the Natural Science Foundation of Zhejiang Province (LR17H180001, LY19H180002), the National Natural Science Foundation of China (51433005, 81900909), and the Australian Research Council (CE140100003).

REFERENCES

(1) Chakrabarti, A.; Das, A.; Mandal, J.; Shivaprakash, M. R.; George, V. K.; Tarai, B.; Rao, P.; Panda, N.; Verma, S. C.; Sakhuja, V. The Rising Trend of Invasive Zygomycosis in Patients with Uncontrolled Diabetes Mellitus. *Med. Mycol.* **2006**, *44*, 335−342.
(2) Mollazadegan, K.; Kugelberg, M.; Montgomery, S. M.; Sanders, D. S.; Ludvigsson, J.; Ludvigsson, J. F. A Population-based Study of the Risk of Diabetic Retinopathy in Patients with Type 1 Diabetes and Celiac Disease. *Diabetes Care* **2013**, *36*, 316−321.
(3) Boudina, S.; Abel, E. D. Diabetic Cardiomyopathy, Causes and Effects. *Rev. Endocr. Metab. Disord.* **2010**, *11*, 31−39.
(4) Wang, J. Electrochemical Glucose Biosensors. *Chem. Rev.* **2008**, *108*, 814−825.
(5) Saei, A. A.; Dolatabadi, E. J. N.; Najafi-Marandi, P.; Abhari, A.; Guardi, M. Electrochemical Biosensors for Glucose based on Metal Nanoparticles. *TrAC, Trends Anal. Chem.* **2013**, *42*, 216−227.
(6) Taormina, C. R.; Baca, J. T.; Ashe, S. A.; Grabowski, J. J.; Finegold, D. N. Analysis of Tear Glucose Concentration with Electrospray Ionization Mass Spectrometry. *J. Am. Soc. Mass Spectrom.* **2007**, *18*, 332−336.
(7) Geim, A. K.; Novoselov, K. S. The Rise of Graphene. *Nat. Mater.* **2007**, *6*, 183−191.
(8) Zhao, B.; Dong, K.; Lin, M.; Dong, G.; Shan, S.; Lawson, T.; Yan, L.; Zhang, W.; Shi, B.; Chou, S.; Baker, M. S.; Liu, Y. A transferrin triggered pathway for highly targeted delivery of graphene-based nanodrugs to treat choroidal melanoma. *Adv. Healthcare Mater.* **2018**, *7*, 1800377.

DOI: 10.1021/acsbiomaterials.9b01149
ACS Biomater. Sci. Eng. XXXX, XXX, XXX−XXX

(9) Zhu, Z.; Garcia-Gancedo, L.; Flewitt, A. J.; Xie, H.; Moussy, F.; Milne, W. I. A Critical Review of Glucose Biosensors based on Carbon Nanomaterials: Carbon Nanotubes and Graphene. *Sensors* **2012**, *12*, 5996−6022.
(10) Wang, Y.; Shao, Y.; Matson, D. W.; Li, J.; Lin, Y. Nitrogen-doped Graphene and Its Application in Electrochemical Biosensing. *ACS Nano* **2010**, *4*, 1790−1798.
(11) Zhang, W.; Chen, C.; Yang, D.; Dong, G.; Jia, S.; Zhao, B.; Yan, L.; Yao, Q.; Sunna, A.; Liu, Y. Optical Biosensors based on Nitrogen-doped Graphene Functionalized with Magnetic Nanoparticles. *Adv. Mater. Interfaces* **2016**, *3*, 1600590.
(12) Sheng, Z.; Zheng, X.; Xua, J.; Bao, W.; Wang, F.; Xia, X. Electrochemical Sensor based on Nitrogen doped Graphene: Simultaneous Determination of Ascorbic Acid, Dopamine and Uric Acid. *Biosens. Bioelectron.* **2012**, *34*, 125−131.
(13) Guo, H.; Peng, S.; Xu, J.; Zhao, Y.; Kang, X. Highly Stable Pyridinic Nitrogen Doped Graphene Modified Electrode in Simultaneous Determination of Hydroquinone and Catechol. *Sens. Actuators, B* **2014**, *193*, 623−629.
(14) Zitolo, A.; Goellner, V.; Armel, V.; Sougrati, M. T.; Mineva, T.; Stieva, L.; Fonda, E.; Jaouen, F. Identification of Catalytic Sites for Oxygen Reduction in Iron- and Nitrogen-doped Graphene Materials. *Nat. Mater.* **2015**, *14*, 937−942.
(15) Shao, Y.; Zhang, S.; Engelhard, M. H.; Li, G.; Shao, G.; Wang, Y.; Liu, J.; Aksay, I. A.; Lin, Y. Nitrogen-doped Graphene and Its Electrochemical Applications. *J. Mater. Chem.* **2010**, *20*, 7491−7496.
(16) Xing, T.; Zheng, Y.; Li, L.; Cowie, B. C.; Gunzelmann, D.; Qiao, S.; Huang, S.; Chen, Y. Observation of Active Sites for Oxygen Reduction Reaction on Nitrogen-doped Multilayer Graphene. *ACS Nano* **2014**, *8*, 6856−6862.
(17) Dou, S.; Shen, A.; Tao, L.; Wang, S. Molecular Doping of Graphene as Metal-free Electrocatalyst for Oxygen Reduction Reaction. *Chem. Commun.* **2014**, *50*, 10672−10675.
(18) Zheng, Z.; Huang, L.; Yan, L.; Yuan, F.; Wang, L.; Wang, K.; Lawson, T.; Lin, M.; Liu, Y. Polyaniline Functionalized Graphene Nanoelectrodes for the Regeneration of PC12 Cells via Electrical Stimulation. *Int. J. Mol. Sci.* **2019**, *20*, 2013.
(19) Sheng, Z.; Shao, L.; Chen, J.; Bao, W.; Wang, F.; Xia, X. Catalyst-free Synthesis of Nitrogen-doped Graphene via Thermal Annealing Graphite Oxide with Melamine and Its Excellent Electrocatalysis. *ACS Nano* **2011**, *5*, 4350−4358.
(20) Wang, C.; Zhou, Y.; He, L.; Ng, T.-W.; Hong, G.; Wu, Q.; Gao, F.; Lee, C.-S.; Zhang, W. In Situ Nitrogen-doped Graphene Grown from Polydimethylsiloxane by Plasma Enhanced Chemical Vapor Deposition. *Nanoscale* **2013**, *5*, 600−605.
(21) Long, D.; Li, W.; Ling, L.; Miyawaki, J.; Mochida, I.; Yoon, S.-H. Preparation of Nitrogen-doped Graphene Sheets by a Combined Chemical and Hydrothermal Reduction of Graphene Oxide. *Langmuir* **2010**, *26*, 16096−16102.
(22) Yan, L.; Lin, M.; Zeng, C.; Chen, Z.; Zhang, S.; Zhao, X.; Wu, A.; Wang, Y.; Dai, L.; Qu, J.; Guo, M.; Liu, Y. Electroactive and Biocompatible Hydroxyl-functionalized Graphene by Ball Milling. *J. Mater. Chem.* **2012**, *22*, 8367−8371.
(23) Kaats, G. R.; Michalek, J. E.; Preuss, H. G. Evaluating Efficacy of a Chitosan Product using a Double-blinded, Placebo-controlled Protocol. *J. Am. Coll. Nutr.* **2006**, *25*, 389−394.
(24) Kang, X. H.; Wang, J.; Wu, H.; Aksay, I. A.; Liu, J.; Lin, Y. Glucose Oxidase-gaphene-chitosan Modified Electrode for Direct Electrochemistry and Glucose Sensing. *Biosens. Bioelectron.* **2009**, *25*, 901−905.
(25) Shan, S.; Jia, S.; Lawson, T.; Yan, L.; Lin, M.; Liu, Y. The Use of TAT Peptide-Functionalized Graphene as a Highly Nuclear-Targeting Carrier System for Suppression of Choroidal Melanoma. *Int. J. Mol. Sci.* **2019**, *20*, 4454.
(26) Pan, H.; Liu, L.; Guo, Z.; Dai, L.; Zhang, F.; Zhu, D.; Czerw, R.; Carrol, D. L. Carbon Nanotubols from Mechanochemical Reaction. *Nano Lett.* **2003**, *3*, 29−32.
(27) Jeong, H.-M.; Lee, J.-W.; Shi, W.-H.; Choi, Y.-J.; Shin, H.-J.; Kang, J.-K.; Choi, J.-W. Nitrogen-Doped Graphene for High-Performance Ultracapacitors and the Importance of Nitrogen-Doped Sites at Basal Planes. *Nano Lett.* **2011**, *11*, 2472−2477.
(28) Yan, L.; Wang, Y.; Xu, X.; Zeng, C.; Hou, J.; Lin, M.; Xu, J.; Sun, F.; Huang, X.; Dai, L.; Lu, F.; Liu, Y. Can Graphene Oxide Cause Damage to Eyesight? *Chem. Res. Toxicol.* **2012**, *25*, 1265−1270.

DOI: 10.1021/acsbiomaterials.9b01149
ACS Biomater. Sci. Eng. XXXX, XXX, XXX−XXX